Characteristics of storm time electric fields in the inner magnetosphere derived from Cluster data

H. Matsui,[1] P. A. Puhl-Quinn,[2] J. W. Bonnell,[3] C. J. Farrugia,[1] V. K. Jordanova,[4] Yu. V. Khotyaintsev,[5] P.-A. Lindqvist,[6] E. Georgescu,[7] and R. B. Torbert[1]

Received 10 March 2010; revised 30 June 2010; accepted 16 August 2010; published 20 November 2010.

[1] Storm-time electric fields in the inner magnetosphere measured by Cluster are reported in this study. First, we show two events around the time when *Dst* index is at a minimum. The electric field possibly related to subauroral ion drifts and/or undershielding is measured inside the inner edge of the electron plasma sheet in the eveningside. For the second event observed in the nightside, the electric field is partly related to dipolarization and is considered as inductive. An electric field without coincident magnetic signatures is also observed. Spatial coherence of the electric field is not large when we check multispacecraft data. It is inferred that the electric field in the magnetotail penetrates inside the region 1 current, while it is not clear about the electric field within the region 2 current from our data. Then superposed epoch analyses using 71 storms are performed. Electric fields at $R = 3.5–6R_E$ and less than 25 degrees of magnetic latitudes are enhanced around the minimum *Dst* at all magnetic local times. Electric fields during the recovery phase decay on a time scale shorter than that of *Dst* index, which could be interpreted in terms of the relation between electric field and ring current during that storm phase. AC electric fields are generally larger than DC electric fields, indicating that the former component might play some role in accelerating ring current particles. These results will be useful to update our empirical electric field model.

Citation: Matsui, H., P. A. Puhl-Quinn, J. W. Bonnell, C. J. Farrugia, V. K. Jordanova, Yu. V. Khotyaintsev, P.-A. Lindqvist, E. Georgescu, and R. B. Torbert (2010), Characteristics of storm time electric fields in the inner magnetosphere derived from Cluster data, *J. Geophys. Res.*, *115*, A11215, doi:10.1029/2010JA015450.

1. Introduction

[2] Motion of cold, dense charged particles in the plasmasphere in the direction perpendicular to the magnetic field is mainly determined by $E \times B$ drift [e.g., *Lemaire and Gringauz*, 1998]. Ring current particles are not only affected by gradient B drift and curvature drift but also by $E \times B$ drift [e.g., *Roederer*, 1970]. Electric field is therefore one important parameter to be investigated in the inner magnetosphere. Plasmaspheric and ring current particles show dynamic behavior during storm periods [e.g., *Wolf*, 1983; *Kistler et al.*, 1989; *Carpenter et al.*, 1993; *Kamide et al.*, 1998; *Jordanova et al.*, 2006]. A question naturally arises concerning how the electric fields behave during these storm periods.

[3] *Maynard et al.* [1983] reported plasmaspheric electric fields from the equatorially orbiting ISEE 1 spacecraft. The electric field is enhanced during active periods. *Baumjohann et al.* [1985] showed *Kp* dependence of electric fields at geosynchronous orbit measured by the GEOS 2 electron gun experiment. *Rowland and Wygant* [1998] reported a *Kp* dependence of dawn-dusk electric field in the afternoon to postmidnight local time sectors measured by CRRES. One notable feature is an increasing electric field strength as the spacecraft approaches the Earth. This is opposite from the usual ionospheric shielding of the magnetospheric electric fields. *Wygant et al.* [1998] examined electric fields during storm periods using the same data set. Large electric fields up to magnitudes of 6 mV/m are observed in the eveningside and nightside and are continuous for periods of the order of an hour or more. These electric fields are correlated with decrease of *Dst* index and are effective in accelerating plasma sheet particles drifting earthward. They found large electric fields at $L < 4–5$ rather than $L > 6$. *Ohtani et al.* [2007] used Cluster data to show oscillatory electric fields with a period of ~10 min associated with a sawtooth signature.

[4] There are reports on large electric fields during storms at low altitudes in addition to the observations around the magnetic equator noted above. *Yeh et al.* [1991] reported large electric fields corresponding to subauroral ion drifts (SAID) or subauroral polarization stream (SAPS) in the duskside

[1]Space Science Center, University of New Hampshire, Durham, New Hampshire, USA.
[2]AER, Inc., Lexington, Massachusetts, USA.
[3]Space Sciences Laboratory, University of California, Berkeley, California, USA.
[4]Los Alamos National Laboratory, Los Alamos, New Mexico, USA.
[5]Swedish Institute of Space Physics, Uppsala, Sweden.
[6]Alfvén Laboratory, Royal Institute of Technology, Stockholm, Sweden.
[7]Max-Planck-Institut für Sonnensystemforschung, Katlenburg-Lindau, Germany.

0148-0227/10/2010JA015450

from the Millstone Hill radar and DMSP observations. They measured large, persistent electric fields with a peak at L = 2.3 during periods concurrent with ring current measurement contributed by heavy ions. *Anderson et al.* [2001] reported multispacecraft measurement of SAID by DMSP. *Okada et al.* [1993] reported large electric field measured by Akebono. The electric fields are enhanced at similar locations as the above work during the main and recovery phases. These electric fields are related to plasma depletion outside the plasmapause. Storm-enhanced density (SED) was measured in evening magnetic local times (MLT) [*Foster*, 1993]. They found coexistence of large electric field and enhanced density. This material is considered as circulating from the middle latitudes to the polar cap.

[5] The electric field in the inner magnetosphere shows dynamic behavior during active periods as noted above. It is important to know the magnetotail phenomena in order to understand this electric field. This is because magnetospheric plasma convects earthward from the magnetotail due to magnetic reconnection in that area [*Dungey*, 1961]. *Baumjohann et al.* [1996] reported that storm time substorms have more pronounced dipolarization, Earthward convection, and higher temperature than nonstorm substorms at radial distances of 10–19 R_E. *Schödel et al.* [2002] examined convection in the 10–31 R_E range of the magnetotail during storm periods, in which earthward flux transport increases. However, such amount decreases as a magnetic flux approaches the Earth. Accumulated magnetic flux leads to the dipolarization in the central plasma sheet. *Lui et al.* [2001] discussed two ideas how the magnetotail plasma is transported to the inner magnetosphere and participates in the ring current. One is frequent occurrence of substorms and another is enhanced magnetospheric convection. They argued that both processes are important. *Hori et al.* [2005] examined the storm time electric field at 5–15 R_E from the Earth. They found two types of electric fields: intermittent bursts of fluctuating fields and steady, weak duskward fields. This feature is similar to what *Baumjohann et al.* [1990] and *Angelopoulos et al.* [1994] reported for occurrence of bursty bulk flow (BBF) events, namely a small fraction of data has this feature, although these studies are not limited to storm events. *Sergeev et al.* [1996] reviewed the occurrence of high-speed flows during steady magnetospheric convection (SMC) in the magnetotail. The calculated occurrence rate is not large, which is also similar to the result by *Hori et al.* [2005].

[6] Concerning the region closer to the Earth, ionospheric shielding of magnetospheric convection becomes significant [*Vasyliunas*, 1970] because of the increasing effect of gradient/curvature drift and the magnetosphere-ionosphere (M-I) coupling compared to the magnetotail. Time variability of plasma pressure during the course of a storm leads to variable shielding effect [*Vasyliunas*, 1972; *Southwood and Wolf*, 1978; *Wolf*, 1983; *Blanc and Caudal*, 1985; *Fejer and Scherliess*, 1997; *Peymirat et al.*, 2000; *Garner et al.*, 2004]. When the magnetospheric electric field is increasing, undershielding happens with penetrating electric fields to low L values inside the inner edge of the electron plasma sheet. In contrast, when the magnetospheric electric field is decreasing, dusk-to-dawn electric field is expected to appear because the ionospheric dynamo wind does not immediately catch up with the magnetospheric changes. Another phenomenon near the Earth is persistent, large electric field known as SAID or SAPS [*Galperin et al.*, 1974; *Yeh et al.*, 1991; *Anderson et al.*, 2001; *Foster and Burke*, 2002; *Puhl-Quinn et al.*, 2007; *Nishimura et al.*, 2008]. SAID or SAPS are caused by different drift orbits of plasma sheet electrons and ions, and is enhanced by low conductivity in the ionosphere. This phenomenon depends on geomagnetic activity and is quite common in the duskside, as shown by a statistical study by *Foster and Vo* [2002].

[7] One reason for enhanced electric field in the duskside compared to the dawnside is that plasma sheet ions from the nightside mainly drift duskward, forming partial ring current, part of which is located inside the inner edge of the electron plasma sheet. This ring current is connected to ionospheric electric current through the M-I coupling. Duskside electric field is thus expected to show dynamic behavior such as the above-noted shielding and SAID during active periods.

[8] We are currently developing an inner-magnetospheric electric field (UNH-IMEF) model [*Matsui et al.*, 2008]. The present version is available through a website (http://edi.sr.unh.edu/unh-imef/). Eight years of data from Cluster are used to develop this model and are organized by interplanetary electric field (IEF). The data contributing to this model are mostly acquired during nonstorm periods and [*Jordanova et al.*, 2009] showed that the ring current buildup is underestimated during large storm periods. However, our community is often interested in these extreme periods. There is a need to examine the electric field during storm periods in more detail, as this could lead to future improvement of the model.

[9] As noted above, the electric field is one of the key parameters to be investigated in the inner magnetosphere. The objective of this study is to examine electric fields during storm periods using Cluster data. Although CRRES spacecraft formerly performed measurements in the inner magnetosphere [*Rowland and Wygant*, 1998; *Wygant et al.*, 1998; *Nishimura et al.*, 2008], there are the following six characteristics in Cluster's measurements.

[10] 1. A large amount of data has been acquired since Cluster's launch in 2000 so that a large number of storms are measured. This study involves more storms than the published CRRES studies.

[11] 2. There are two instruments onboard to measure electric fields, electron drift instrument and double probe instrument, both of which are complementary to each other.

[12] 3. This study uses two components of the electric field E_X and E_Y, while some CRRES studies use the dawn-dusk component only.

[13] 4. This study has improved MLT coverage relative to CRRES which did not have electric field measurements in the morning sector.

[14] 5. Interplanetary data are available throughout the Cluster mission, while this was not often the case during the CRESS mission.

[15] 6. The radial coverage of this study using Cluster measurements (mostly 4–5.5R_E) does not include the extremely low L values ($L \sim 2.5$) that the CRRES data do.

[16] We are interested in looking at electric field signatures around the time when *Dst* index is at a minimum,

and first we analyze such two events. The two events were measured in the eveningside and the nightside, respectively. Then, we examine electric fields statistically. The questions we address are as follows. How does the electric field depend on the storm phase at each MLT sector? Is the electric field in the nightside comparable with that in the magnetotail? The Alfvén layer in the eveningside is located farther away from the Earth compared to other MLT sectors and hence the spatial area with shielding and SAID/SAPS overlaps with Cluster's orbits included in this study. It is therefore worthwhile to check how these phenomena are measured in our data. There are not so many reports on electric field observations in the dayside and morningside during geomagnetic storms. After examining the MLT dependence, we compare time sequences of electric field during the course of storms with those of interplanetary and geomagnetic parameters. Because of good coverage of interplanetary data, this type of comparison between the electric field data and the interplanetary data is probably made for the first time in this study. We are also interested in the strength of the AC components relative to DC components. This type of study is expected to be useful to understand dynamics of the plasmasphere and ring current which are partly controlled by the electric field.

[17] This study is organized as follows. The data we use are described in section 2. In section 3, case studies for two events around minimum *Dst* are reported. Statistical analyses are presented in section 4 to answer the above questions. Discussion follows in section 5. The results obtained are compared with previous observations and theories. Finally, conclusions are given in section 6.

2. Data Set

[18] The data mainly used in this study are those acquired by Cluster [*Escoubet et al.*, 2001]. Cluster consists of four spacecraft (SC 1–4) with identical instrumentation and has a polar orbit with a period of 57 h. The apogee is ~20 R_E, while the perigee is ~4 R_E until middle of 2006. After that the perigee is getting closer to the Earth. A fraction of time is inside the inner magnetosphere during an orbit so that data of our interest are obtained only intermittently. We use electric field data from two instruments complementary to each other: the Electron Drift Instrument (EDI) [*Paschmann et al.*, 2001] and a conventional double probe instrument, the Electric Field and Wave (EFW) instrument [*Gustafsson et al.*, 2001]. EDI data were so far analyzed in the inner magnetosphere [*Matsui et al.*, 2003; *Puhl-Quinn et al.*, 2007] and in the polar cap [*Haaland et al.*, 2007; *Förster et al.*, 2007]. EDI data used in this study have a maximum time resolution of 1 s, although there are intermittent data gaps. We take data with all quality but have removed data spikes which are different by more than 10 mV/m from neighboring points because part of this could be unrealistic. The EFW data with 4 s resolution with good quality are obtained from Cluster Active Archive [*Lindqvist et al.*, 2006; *Khotyaintsev et al.*, 2010]. We merge data from both instruments following the procedure noted in *Puhl-Quinn et al.* [2008] as an initial step. Inclusion of EFW data requires at least that one EDI data point exists during each 5 min interval. Then the average offset between EDI and EFW is subtracted from EFW data. In this study, we have modified this procedure. We include EFW data with EFW probe potential between −6 and −2 V, even when there is no EDI data within each 5 min. This EFW data inclusion is based on EFW-EDI data comparison. Nominal offset corrections are applied to EFW data. The electric field data presented in this study are in situ values instead of mapped values unlike [*Matsui et al.*, 2003]. This is because we would like to avoid the ambiguity of the mapping procedure due to the choice of the magnetic field model. Contributions from spacecraft motion and corotation are subtracted. Corotation electric field is mostly 0.5–1 mV/m for the data used in this study.

[19] We also use FluxGate Magnetometer (FGM) data [*Balogh et al.*, 2001] in the case study in order to identify background field and dipolarization signatures. The EDI instrument measures ambient electron counts at an energy of 500 eV or 1 keV in addition to electron drift motion. These data are used to visually find the inner edge of the electron plasma sheet when possible.

[20] We further introduce magnetic field data and plasma data from ACE [*Smith et al.*, 1998; *McComas et al.*, 1998] to identify interplanetary conditions. Geomagnetic parameters analyzed include *Dst*, *Kp*, *AL*, and *AU* indices. The latter two are a provisional version. *SYM-H* indices are introduced to complement *Dst* indices in the case study.

3. Case Studies

[21] In this section, we show two events during which Cluster measurements are taken around minimum *Dst*. This will illustrate electric field behavior during the peak of storms and complement statistical analyses in section 4.

3.1. Eveningside Event on 19 May 2002

[22] Cluster passed through the eveningside inner magnetosphere around the time of minimum *Dst* during a storm on 19 May 2002. Figure 1 shows, from top to bottom, *Dst* and *SYM-H* indices, three components of interplanetary magnetic field (IMF) in geocentric solar magnetospheric (GSM) coordinates, solar wind dynamic pressure, and the *AL* and *AU* indices during 0000–1200 UT. Measured values from ACE are shifted in time using the convection velocity and the spacecraft position as *Matsui et al.* [2003] did. Two vertical lines show an interval within which Cluster data are investigated later. This interval corresponds to when *Dst* and *SYM-H* take minimum values with ~−60 and −70 nT, respectively. IMF B_Z is fluctuating and takes positive values until ~0340 UT. Then it takes negative values and show a minimum value ~−10 nT at ~0450 UT. IMF B_Z recovers to smaller values by ~0900 UT. IMF B_X and B_Y often take negative and positive values, respectively. Solar wind dynamic pressure takes large values >5 nPa until ~0420 UT. After that, the values are a few nPa with a decreasing trend. These are generally higher values than typical. Auroral electrojet shows some activities. Eastward electrojet represented by AU index is enhanced after ~0330 UT and shows a few peaks. Westward electrojet represented by *AL* index starts to strengthen around the same time. There are decreases during the interval in which we will show the Cluster data. After that the *AL* values recover.

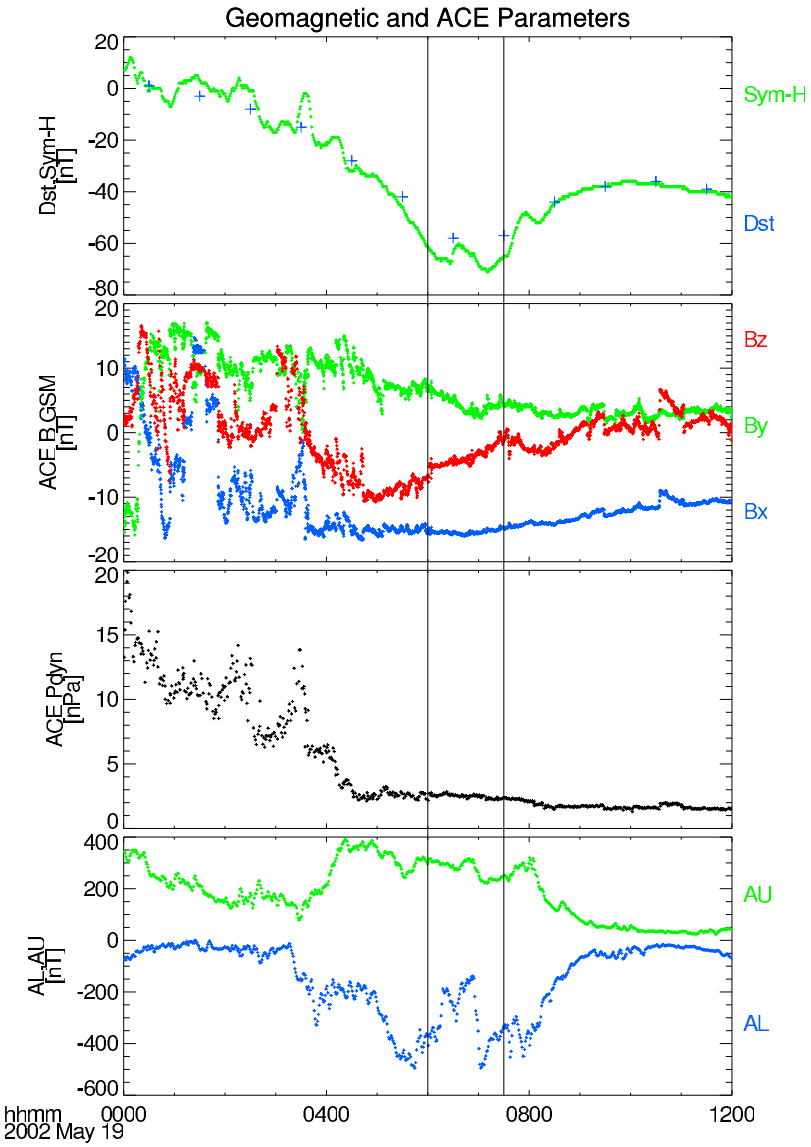

Figure 1. Geomagnetic indices and ACE parameters on 0000–1200 UT, 19 May 2002. *Dst* and *SYM-H* indices, interplanetary magnetic field (IMF), solar wind dynamic pressure, and *AL* and *AU* indices are shown from top to bottom. The two vertical lines indicate the time interval within which we show Cluster data in Figure 2.

[23] Cluster measurements at 0600–0730 UT, 19 May 2002 are shown in Figure 2. At this time, SC 1 is located around the magnetic equator with the radial distance of 4.4–4.6 R_E. The spacecraft continuously stays inside the inner edge of the electron plasma sheet during the period bounded by the two vertical lines. The inner edge is identified by the decrease of 1 keV electron counts in the bottom. The electric field components in the top show a fluctuating signature in the plasma sheet up to 0624 UT. After that the spacecraft stays inside the inner edge. The electric field is in the order of 1 mV/m with small fluctuating components. The direction is outward and westward and is consistent with that of SAPS. The size of the electric field is enhanced at 0643 UT and the electric field changes sign soon after that. The plasma sheet electrons are seen at 0646 UT. Subsequently, the location of inner edge passes through the spacecraft location intermittently. The electric field simultaneously changes its sign. After 0651 UT, the spacecraft is often inside the plasma sheet, where the electric field is again variable. We have also checked the measurements made by other Cluster spacecraft. At this time, the spacecraft separation is small with <100 km in the direction perpendicular to the magnetic field. The time series do not change much between spacecraft.

[24] The large electric field inside the inner edge can be interpreted in the global context. The ring current is a primary driver of under/overshielding so that the spatial relationship between the electric field and the ring current is important. [*Nishimura et al.*, 2008] found that the electric field increases within 30 s of the substorm onset. The ring current in the inner edge is transported and energized by this electric field. The SAPS electric field is then enhanced and localized due to the current closure through the ionosphere

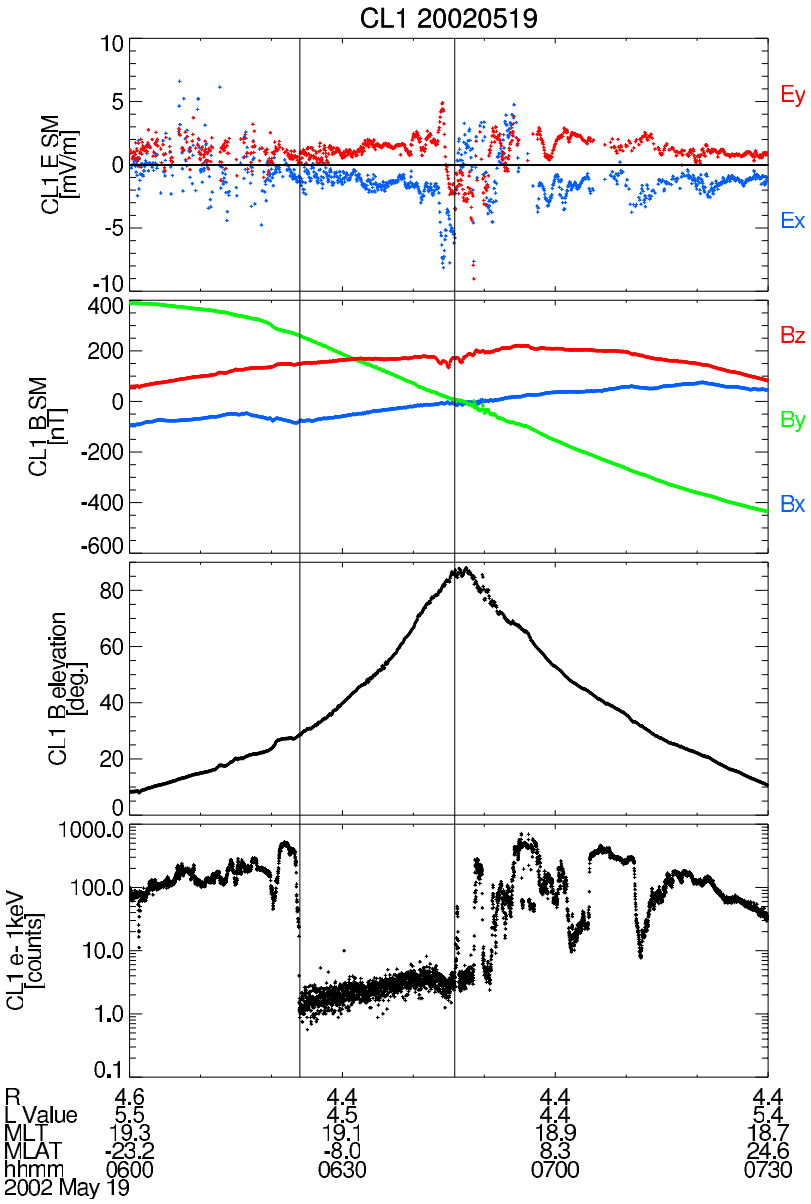

Figure 2. Cluster measurements from SC 1 at 0600–0730 UT, 19 May 2002. Two components of electric field in SM coordinates, three components of magnetic field, elevation angle of magnetic field, and 1 keV electrons with a pitch angle of 90 degrees are shown. Following quantities of the spacecraft location are indicated in the bottom: radius, *L* value, MLT, and MLAT. The two vertical lines show where Cluster continuously stays inside the inner edge of the electron plasma sheet.

with low conductivity. The SAPS electric field is located in a charge-accumulated region between the earthward edge of the ring current and the plasma sheet. The charge accumulation occurs due to positive charge of ring current ions.

[25] Finally, it should be mentioned that the electric field during this time interval mostly comes from the EFW measurement. The exception is 0718–0730 UT (Figure 3). During this interval both EDI and EFW data show a similar trend.

3.2. Nightside Event on 18 February 2005

[26] We then examine an event in which Cluster was in the nightside. Figure 4 shows geomagnetic and interplanetary parameters from 1800 UT, 17 February 2005 to 0600 UT, 18 February. The interval corresponds to the sheath region of an interplanetary coronal mass ejection (ICME) lasting from 1400 UT, 18 February to 0600 UT, 19 February. The two vertical lines indicate the interval in which we will show Cluster data in Figure 5. *Dst* and *SYM-H* indices shown in the top indicate storm main phase starts around 2300 UT. The period to present Cluster observations corresponds to the main phase a few hours prior to the minimum *Dst* or *SYM-H* of ~−85 or −95 nT, respectively. IMF B_Z fluctuates strongly at ~2200–2300 UT. Then, it takes mostly negative values. The minimum IMF B_Z reaches ~−20 nT around 0100 UT. After that the values increase and fluctuate. The dynamic pressure shows large rise to 10 nPa at ~2300 UT caused by arrival of an interplanetary shock driven by the ICME. The increase continues for ~10 min. Then, the values

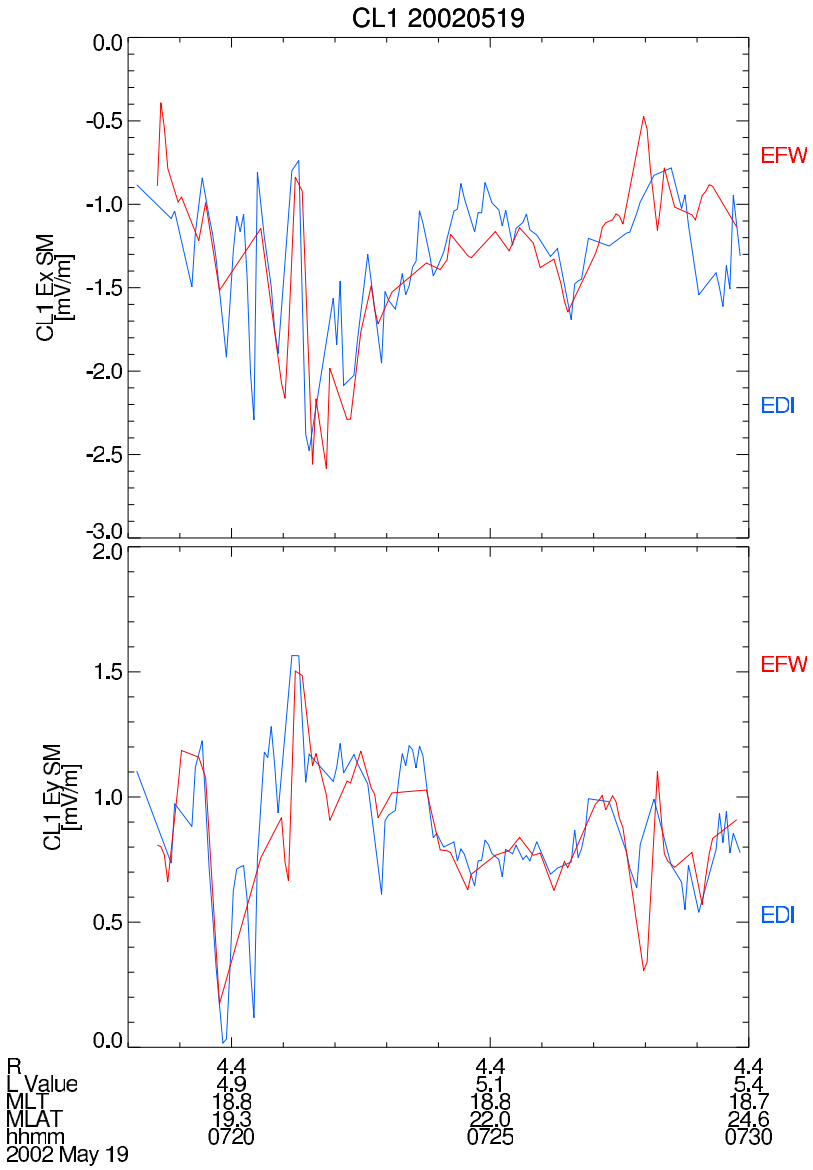

Figure 3. Comparison of electric fields measured by EDI and EFW. EDI and EFW data are shown by blue and red traces, respectively. Both data follow similar time series.

decrease to ~5 nPa. Another transient increase is found at ~0025 UT. The auroral electrojet shows a dynamic behavior during this interval especially in *AL* values. The *AL* values start to decrease around the time when IMF B_Z turns to large negative values <~−10 nT. The values gradually decrease including a sporadic decrease at ~0010 UT and peaks at −1500 nT at ~0120 UT. After that the values increase and approach a quiet level. The *AU* values show a peak of 360 nT. Time variability is not as large as *AL* values.

[27] Cluster measurements by SC 3 during part of the interval discussed are shown in Figure 5. This period corresponds to main phase of the storm. Electric field data during this interval are all measured by EFW. In Figure 5, two notable features are (1) a large electric field pulse coincident with a dipolarization signature and (2) a large electric field after that, although the amplitude gets smaller.

[28] At 0015 UT, the magnetic elevation angle (third frame) increases from 34 deg. to 41 deg. within 1 min. Simultaneously a large negative E_Y value with ~−15 mV/m is observed. Since the variations in magnetic field and electric field coexist with a similar time scale, this electric field is likely to be inductive. This large electric field is perhaps related to the sporadic decrease of the *AL* index at ~0010 UT. If the magnetic elevation increase was caused by an increase of solar wind dynamic pressure, the value should rather decrease in the nightside [e.g., *Wing and Sibeck*, 1997]. Hence this possibility is unlikely. Just close to the end of the dipolarization, there is a bipolar E_Y variation with an amplitude of 30 mV/m, which seems to be also inductive because it is accompanied by a variation in magnetic field with a similar time scale. The magnetic field line shifted poleward moves back a little bit to the equator.

[29] After the dipolarization, a moderate size of electric field <~10 mV/m is observed. The electric field is not steady but fluctuating. The mean value of E_X is positive. The electric field is not inductive because no significant mag-

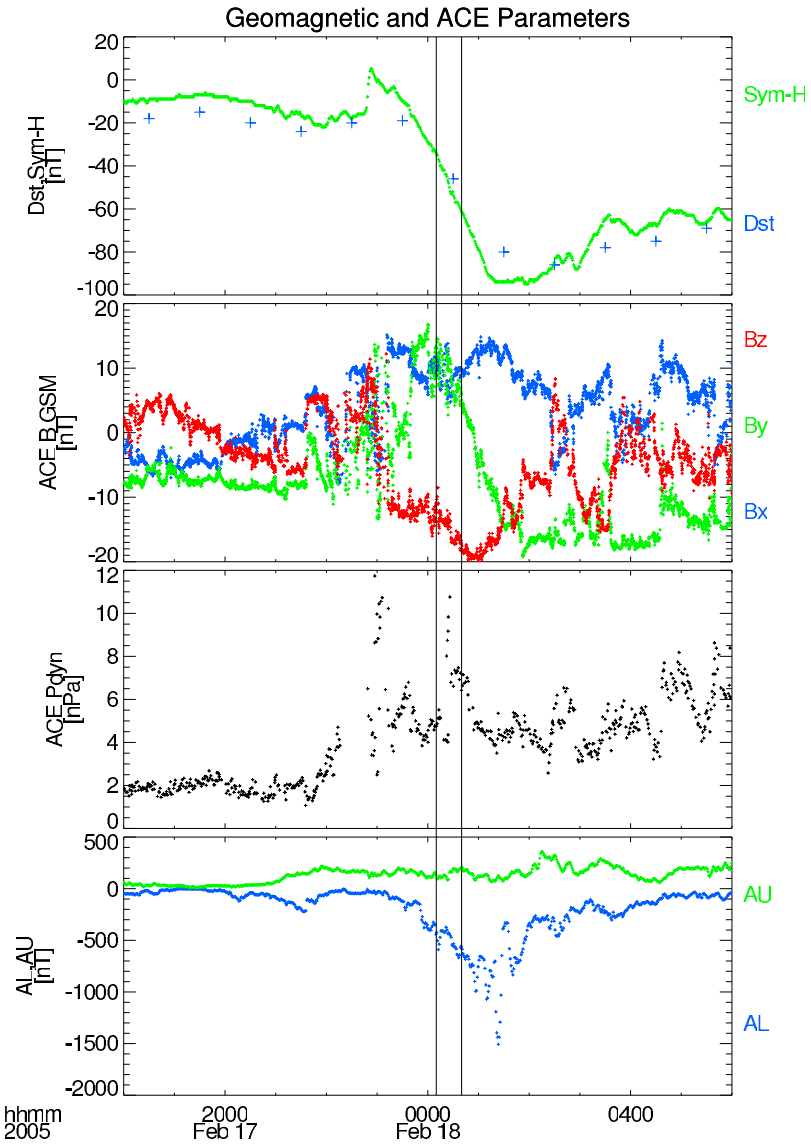

Figure 4. Geomagnetic indices and ACE parameters from 1800 UT, 17 February 2005 to 0600 UT, 18 February. The quantities plotted in Figure 4 are the same as Figure 1. The two vertical lines indicate the time interval within which we show Cluster data in Figure 5.

netic variations other than those of background dipole components are seen. Measurement of this type of electric field which is not simultaneous with dipolarization is not inconsistent with [*Angelopoulos et al.*, 1992], in which bursty bulk flow is mostly, but not completely, coincident with dipolarization. It should also be noted for this event that the spacecraft continuously stayed in the plasma sheet because there are always electron counts at 1 keV (bottom).

[30] One unique feature of Cluster measurements is that they are made at four spacecraft. Relative distance between each spacecraft during this event is shown in Figure 6. Here locations of SC 1, 2, 3, and 4 are plotted with black, red, green, and blue asterisks, respectively. Each spacecraft is separated by 800–5000 km. The separation is especially large in the Z direction. The separation is an order of magnitude larger than that of the previous example on 19 May 2002 so that the measured values are not the same at the various spacecraft. As seen in Figure 6, SC 3 is located at an outermost L shell and then SC 2, 1, and 4 in this order. SC 1 is closest to the magnetic equator.

[31] Figure 7 shows electric field and magnetic elevations from the four spacecraft. From top to bottom, the L values of spacecraft locations decrease. Vertical lines in each frame show possible time of dipolarization, although it is hard to identify such time at inner spacecraft. The dipolarization signature is especially clear at SC 3 as we have already discussed above. This signature is also measured by SC 2, although it is weaker there. It is harder to recognize the dipolarization signature at the inner two spacecraft, SC 1 and 4. This is also true for the inductive electric field. The spatial coherence between measurement at different spacecraft is not high.

[32] Propagation of dipolarization front may be determined using spacecraft positions and timing differences of

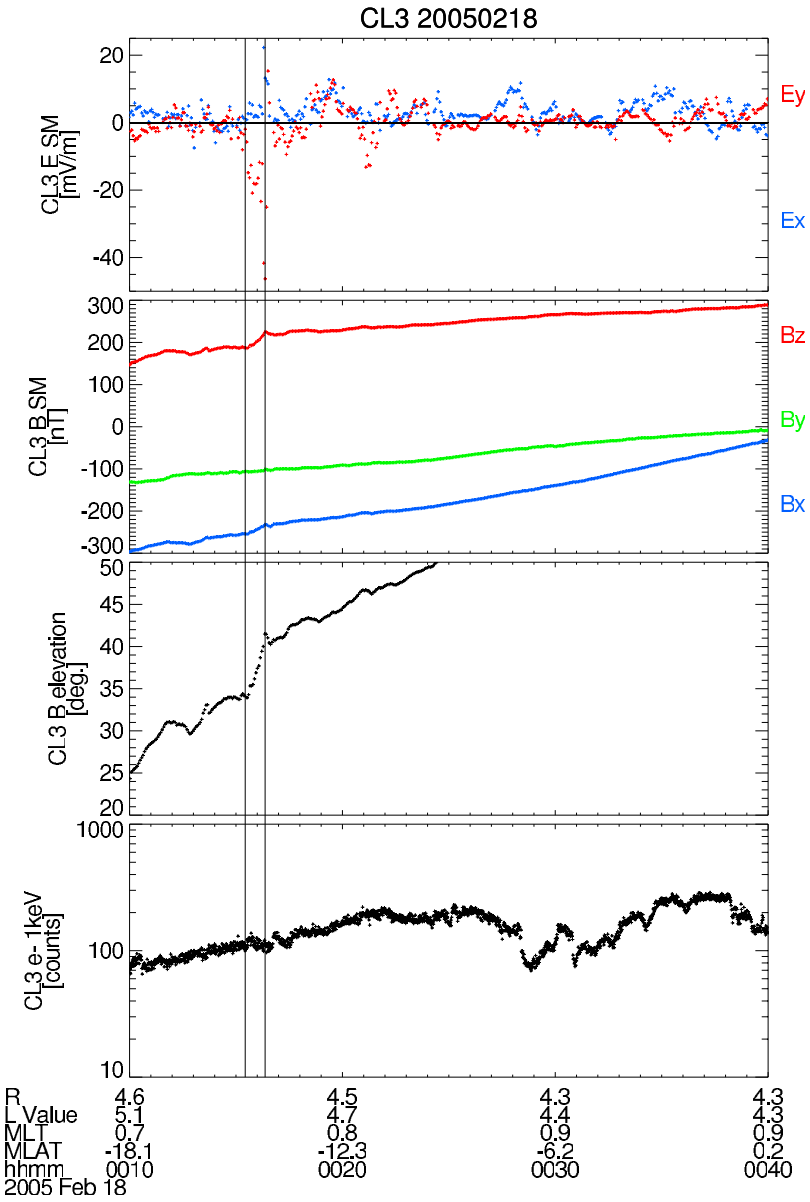

Figure 5. Cluster measurements from SC 3 on 0010–0040 UT, 18 February 2005. The quantities plotted are the same as in Figure 2. The spacecraft location is indicated in the bottom. The two vertical lines show an interval during which Cluster measured an increase of magnetic elevation angle, namely dipolarization.

the front arrival between spacecraft. The front seems to propagate in the $-Z$ direction away from the magnetic equator. It should be noted that this result is not so robust. This is because the dipolarization front is hard to be identified for SC 1 and 4. In addition, spatial homogeneity is not satisfied because of curved magnetic field geometry between spacecraft (Figure 6). There are two possible interpretations about the suggested propagation path of the dipolarization front. The first is that the dipolarization front originated in the magnetotail initially propagates earthward and then along the magnetic field line toward the ionosphere. Second one is that the front is propagating toward larger L value. We have another tool to check the direction of the propagating front. Poynting flux of the dipolarization front is calculated and is directed earthward and away from the equator at SC 3. The former possibility is therefore likely.

[33] After the dipolarization signature is measured, there are large electric fields at all spacecraft locations. These time series are not coherent between different spacecraft. In summary, we can see a variable feature of electric fields both in time and space during this event.

4. Statistical Analyses

4.1. Database

[34] We analyze Cluster electric field data for 8 years between 2001 and 2008. EDI data for SC 1 and 3 are taken between February 2001 and September 2008, while those for SC 2 are taken until April 2004. SC 4 does not operate EDI during most of the mission. EFW data we use are until the end of 2005 for SC 1–3. Five minute averages are calculated to perform statistics after merging EDI and EFW

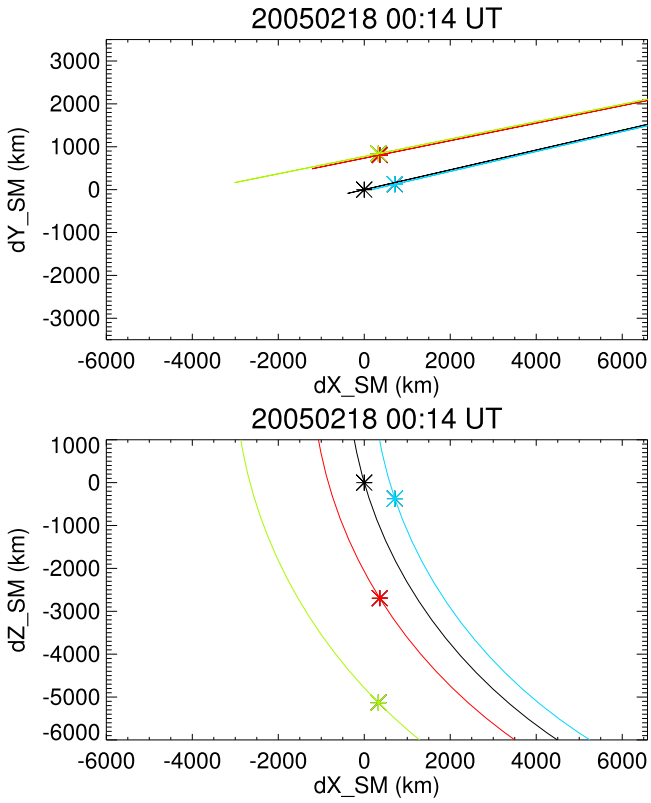

Figure 6. Locations of four Cluster spacecraft in SM coordinates relative to that of SC 1 at (−4.3, −1.0, 0.4) R_E at 0014 UT, 18 February 2005. (top and bottom) Projections onto the *X*-*Y* and *X*-*Z* planes, respectively. Locations of SC 1, 2, 3, and 4 are plotted with black, red, green, and blue colors, respectively. Dipole magnetic field lines threading each spacecraft location are shown as a reference.

data. A spatial range examined is $3.5 < R < 6\ R_E$, $|MLAT| <$ 25 degrees, and full MLT, where R is the geocentric distance of the spacecraft. Then we perform a superposed epoch analysis with the zero epoch when *Dst* index takes a minimum value during the course of a storm. In our study, a storm is picked at when minimum *Dst* values <−50 nT are constant for >72 h. The storm interval is defined as when *Dst* values are continuously less than 20% of the minimum *Dst* value. The periods before and after minimum *Dst* correspond to main and recovery phases, respectively. We then visually inspect time profiles of *Dst* index during each storm to ensure there is a single minimum *Dst* value. Otherwise, events are not included in the database. We have obtained 71 storms with this procedure. Dependence of electric fields on epoch time is then examined for each MLT sector divided into four (each MLT sector has a 6 h width).

[35] Data distribution in our database is presented between −12 and 60 h from zero epoch in Figure 8. We have some amount of data during these intervals. Data are often taken at $4 < R < 5.5\ R_E$. There are not many data points at $R < 4\ R_E$ because Cluster's perigee is located at ~4 R_E until middle of 2006. Absolute values of magnetic latitudes (MLAT) of spacecraft positions often exceed 25 degrees at $R > 5.5\ R_E$. Data are distributed throughout the plot organized by MLT, although there are often regions with no data. Such an example is eveningside at >48 h from zero epoch. The spatial resolution of MLT of 6 h chosen above would be therefore one possible compromise. Blue points in Figure 8 indicate where the spacecraft were inside the inner edge of the electron plasma sheet. Each inner edge is identified by visual inspection of ambient electron counts at 500 eV or 1 keV with a pitch angle of 90 degrees measured by EDI. The points are commonly located in the afternoonside, which is expected from the shape of the Alfvén layer [e.g., *Ejiri*, 1978].

[36] Availability of 5 min data in our database is shown in Figure 9. The availability is defined as number of 5 min intervals with electric field data divided by number of 5 min intervals with EDI and/or EFW in operation. Data availability is often >80% except a few cases. There is not much dependence on MLT. Data gaps are caused by no return beams emitted from electron guns on EDI or the criterion on spacecraft potential to pick EFW data.

4.2. Electric Fields Sorted by Epoch Time

[37] Figure 10 shows 5 min averages of electric fields sorted by epoch time. 6 h averages in epoch time calculated from 5 min averages are shown by blue lines with error bars representing standard deviations. Figures 10a–10d correspond to results at four different MLT ranges. Red and black points in Figure 10d represent results in the premidnight and postmidnight, respectively.

[38] Figure 11 summarizes the electric fields around minimum *Dst* (within 3 h from minimum *Dst*) in order to help understanding the discussion below. Average electric fields for each MLT sector are plotted at average spacecraft locations.

[39] Figure 10a corresponds to statistical results at 3–9 MLT. Large electric fields of a few mV/m are measured during the main phase just before the zero epoch. This is contributed by an event at ~9 MLT. These electric fields are directing inward, indicating plasma flow toward later MLT. The electric fields are fluctuating so that the standard deviation is large. After that, the electric field is not so large with magnitudes <1 mV/m except for some spikes around 24 h from zero epoch. These points are contributed by one event with large *AL* values and hence possibly with magnetotail activity.

[40] Figure 10b shows a result at 9–15 MLT. Again enhanced electric field is measured around zero epoch. Both E_X and E_Y components are positive, indicating flow is outward and westward. The fluctuation is large. There are often cases with the magnitude <1 mV/m even around zero epoch. The size of the electric field is getting smaller during the recovery phase.

[41] Figure 10c shows a result at 15–21 MLT. Electric field is enhanced around zero epoch with negative E_X and positive E_Y, indicating plasma is moving outward and westward toward the magnetopause. The fluctuating component is large. Signs of both E_X and E_Y sometimes get reversed. The event presented in Figure 2 contributes to this large, fluctuating electric field. As noted in the case study, SAPS is measured during a part of time. After that, electric field is getting smaller during the recovery phase. We have shown in Figure 8 that spacecraft are often located inside the inner edge of the electron plasma sheet at this MLT range. E_Y is positive throughout the period possibly measuring SAPS, although the size is small <1 mV/m. The electric fields sometimes take larger values sporadically. One such

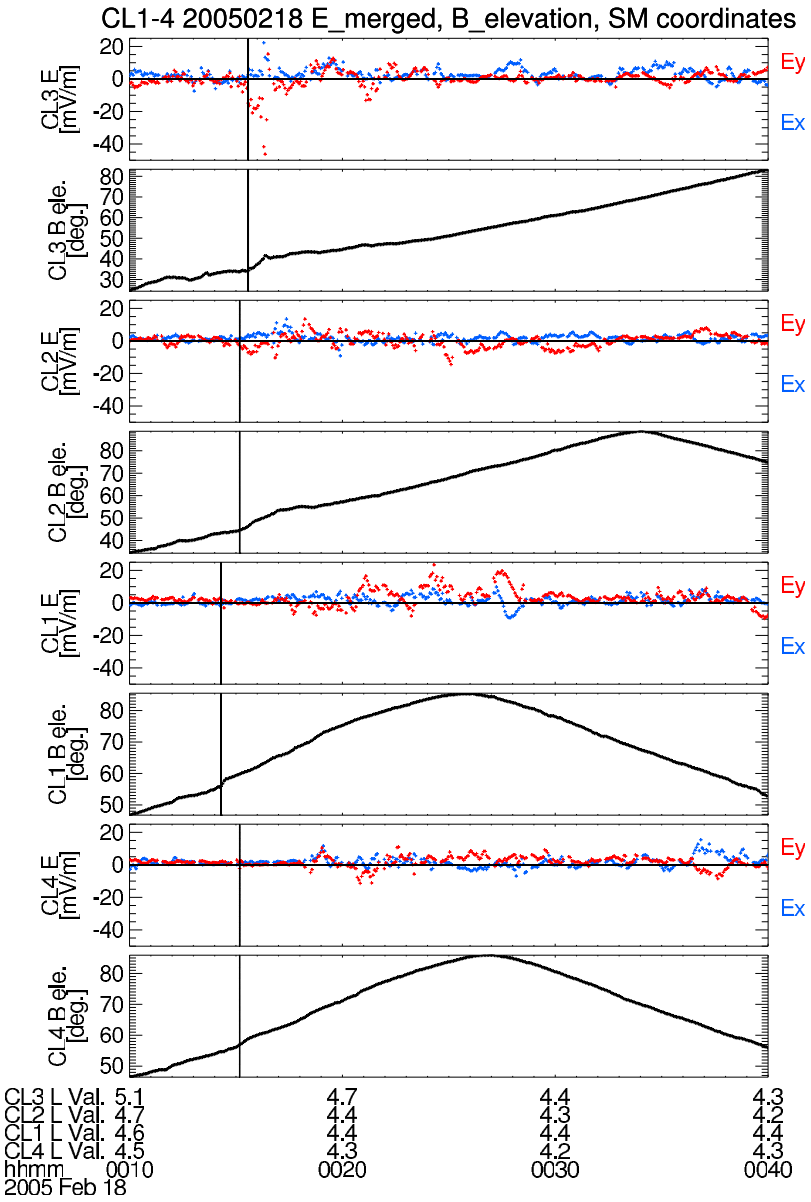

Figure 7. Electric field and magnetic elevation angle measured by four Cluster spacecraft on 0010–0040 UT, 18 February 2005. The L values of spacecraft location decrease from top to bottom. Vertical lines indicate where a dipolarization is likely to start at each spacecraft. Scales of electric fields are adjusted to be the same between spacecraft. L values of each spacecraft location are noted in the bottom.

example at 40 h from zero epoch is caused by an activity with continuously negative values of *AL* index (~−400 nT).

[42] Figure 10d shows electric fields at 21–3 MLT. E_X is positive right around zero epoch. E_Y is on average positive at the same time but fluctuating to change polarity often. We have examined one such event in section 3.2. There are two more events around zero epoch. All three events have large electric fields. *AL* decreases and increases of magnetic elevations are found, although the exact timing does not always match between the increase of magnetic elevations and large electric fields. Some of the electric fields are inductive and others are not. The time scale of fluctuating component is typically less than several minutes, which is not the same as the time scale of undulations or ripples (about several 10s min) [*Goldstein et al.*, 2005]. Amplitudes of electric fields get smaller during the recovery phase. The sign of E_X turns to negative in the premidnight shown by red crosses, while it is continuously positive in the postmidnight shown by black crosses. E_Y is positive throughout the recovery phase.

4.3. Relation of Electric Fields to Geomagnetic and Interplanetary Parameters

[43] Superposed epoch analysis of various geomagnetic and interplanetary parameters during 71 storms are shown with that of E_Y components measured by Cluster in Figure 12. Each parameter is averaged every 3 h in epoch time and shown with standard deviations. E_Y components from Cluster are averaged for a whole MLT range. Superposed epoch analysis of other parameters only includes data when there are Cluster measurements. Each parameter shows a clear

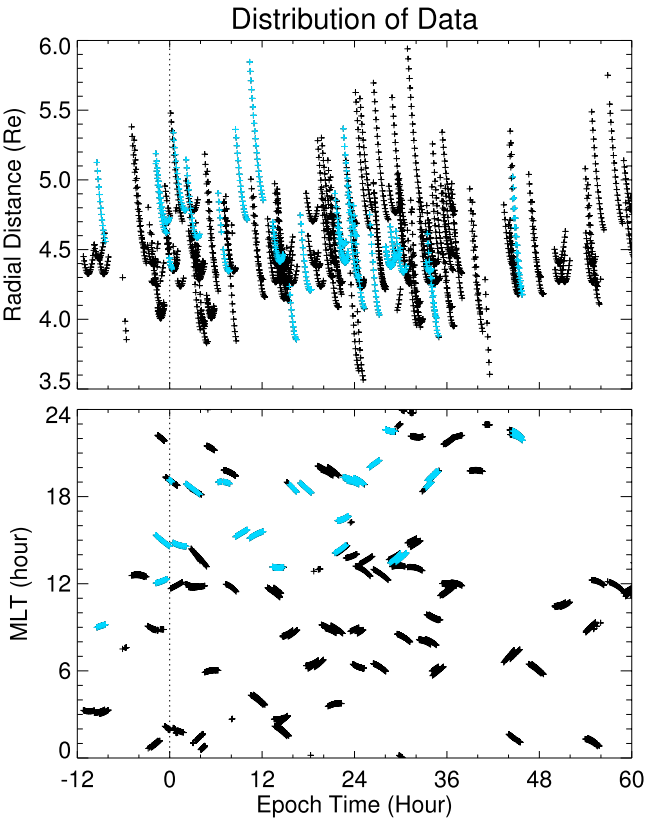

Figure 8. Data distribution in our database. (top and bottom) Radial distance and MLT sorted by epoch time, respectively. The blue points indicate where spacecraft are inside the inner edge of the electron plasma sheet.

maximum or minimum during the main phase similar to [*Zhang et al.*, 2006]. The magnitudes decay in time during the recovery phase. IMF B_Z component quickly turns from negative to positive after zero epoch. *AL* index, IEF, and electric field measured by Cluster recover with a time scale of 9–12 h. It should be noted that IEF is defined here as $V\sqrt{B_Y^2 + B_Z^2}\ \sin^2(\theta/2)$, where V is the solar wind speed, B_Y and B_Z are Y and Z components of IMF, and θ is the IMF clock angle, $\tan^{-1}(B_Z/B_Y)$. The local time dependence of recovery time for Cluster's electric field is not so clearly seen, although electric field in the nightside tends to recover with a longer time scale (figure not shown). *Dst*, *Kp* and *AU* indices recover to a moderate value after ~12 h, although they do not recover to quiet values since then. Concerning this slow *Dst* recovery, one possible reason lies in the event selection procedure in which *Dst* is <20% of minimum values during a storm period defined.

[44] When we calculate E_Y components from Cluster divided by IEF, merging efficiency of IEF into the magnetosphere can be estimated. The values calculated from 6 h averages show a local time dependence (figure not shown). The value in the eveningside is 0.30 on average, while the values in other MLT ranges are 0.11–0.15. There is an extreme IEF value ~25 mV/m for an event in the nightside on 31 March 2001. In this case, the efficiency decreases to 0.05 possibly corresponding to saturation. *Hairston et al.* [2003] estimated saturation of polar cap potential on the same date and our results are qualitatively consistent with theirs.

4.4. Standard Deviation of Electric Fields

[45] The sum of the standard deviations of electric fields for all three components are calculated and shown in Figure 13. The results for four MLT sectors are presented in each frame. Standard deviations calculated correspond to high- and low-frequency fluctuations. High-frequency fluctuations (black points) are standard deviations to calculate 5 min averages from 4 s data. We can see high-frequency fluctuations take values as large as several mV/m occasionally. When we have calculated 6 h averages of this high-frequency fluctuations (blue points), the values are often less than 1 mV/m. This value is comparable to the low-frequency fluctuations (green points), which are standard deviations to calculate 6 h averages in epoch time from 5 min electric fields. Average DC electric field values for 6 h are plotted by red points for comparison. DC fields are generally smaller than AC fluctuations for both high- and low-frequency components, indicating a transient nature of electric fields. Concerning epoch time dependence of fluctuating components, there is an increase around zero epoch at 21–3 MLT. The maximum value is ~20 mV/m, which is largest within the statistical domain. This large fluctuating component is partly contributed by dipolarization events or transient electric fields around the dipolarization as we discussed in section 3.2. It should also be noted that low-frequency fluctuations are contributed by variability between different storm events. We have not normalized each quantity by a storm size which can be defined by the strength of minimum *Dst* values. This limits further interpretation of the low-frequency components. Nonetheless, the vortex-like velocity variations with a period of several minutes reported by *Zong et al.* [2009] might contribute to this low-frequency fluctuations.

5. Discussion

[46] We have examined storm time electric fields based on event studies and statistical studies. Some of the key measured features are discussed in this section: (1) large electric field around zero epoch at each MLT sector, (2) decay of

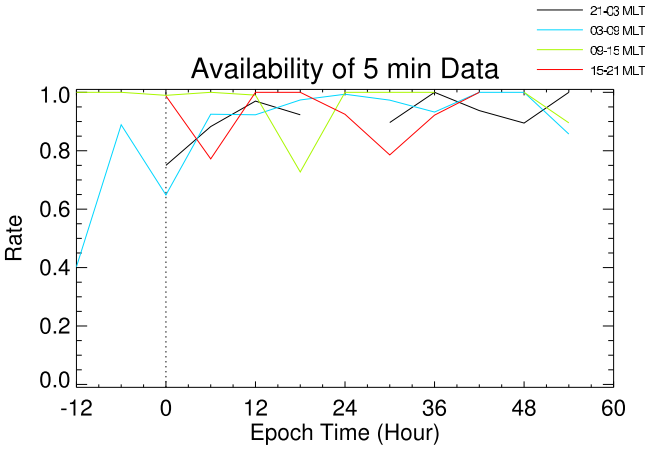

Figure 9. Availability of 5 min data in our statistics for four different MLT ranges.

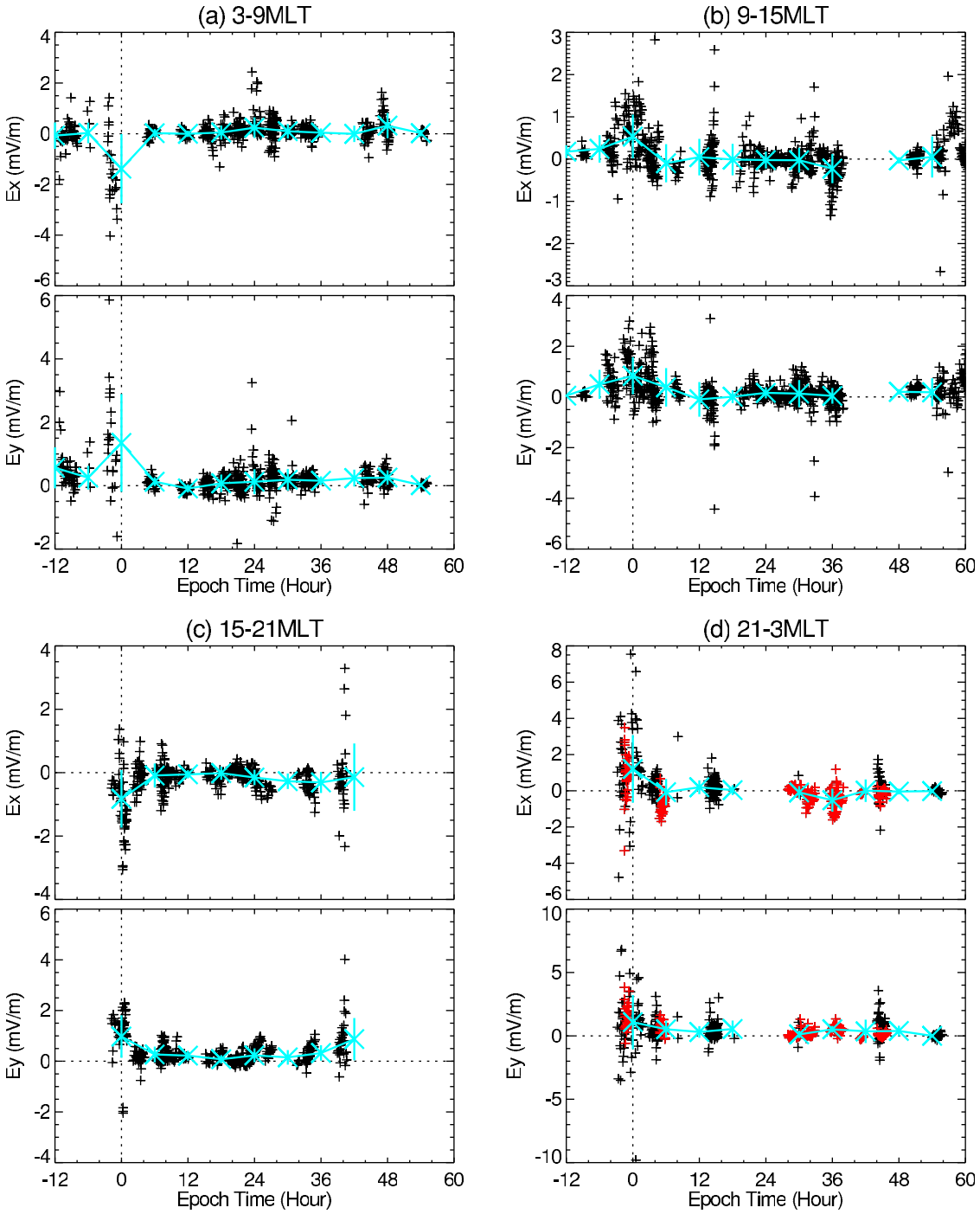

Figure 10. Superposed epoch analysis of two components of electric fields in (a) 3–9 MLT, (b) 9–15 MLT, (c) 15–21 MLT, and (d) 21–3 MLT. Five minute average values are plotted with black points; 6 h averages in epoch time calculated from 5 min averages are shown with blue lines. Standard deviations to calculate 6 h averages are indicated by error bars. Premidnight and postmidnight data in Figure 10d are plotted in red and black colors, respectively.

electric field strength during recovery phase, (3) AC electric field relative to DC electric field, (4) different dipolarization signatures between spacecraft and subsequent large electric fields, and (5) variation of electric fields in the premidnight during the course of storms.

5.1. Large Electric Field Around Zero Epoch

[47] *Wygant et al.* [1998] reported CRRES measurements of dawn-dusk electric field of the order of several mV/m at $L < 7$. These magnitudes of electric fields are consistent with 5 min values of electric fields from our measurements but

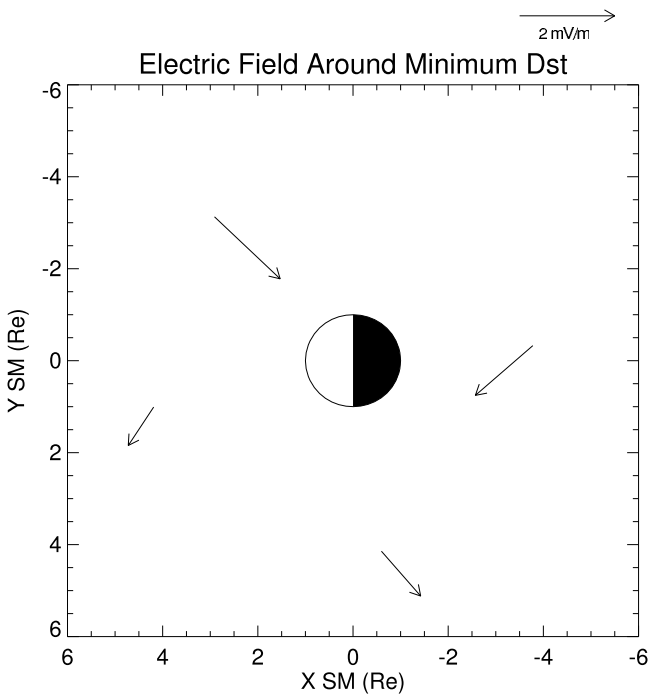

Figure 11. Summary of electric field around the minimum *Dst* between −3 and 3 h from the epoch time. Average electric fields for each MLT sector are plotted as vectors starting at average spacecraft locations. The scale of the electric field is noted in the top right frame.

somewhat larger than 6 h values in the nightside around zero epoch ($E_Y \sim 1.1$ mV/m). The latter discrepancy is possibly caused by radial distance of measurements of large electric fields made by CRRES earthward of Cluster's orbits. In a simulation using Rice Convection Model (RCM) by [*Garner et al.*, 2004], large electric fields with $E_X \sim 3$ mV/m appear in the nightside at $L < 4$ around minimum *Dst*. This is again consistent with the above consideration.

[48] Superposed epoch analysis of bursty bulk flow events during storm periods is reported by [*Baumjohann et al.*, 1996] in the magnetotail at radial distances of 10–19 R_E. The typical flow speed ~100 km/s and the magnetic pressure ~0.6 nPa they reported lead to $E_Y \sim 4$ mV/m. This size is consistent with our measurements of 5 min averages. Bursty bulk flow is observed sporadically, which is consistent with occasional increase of the 5 min values in our measurements.

[49] We can compare our measurements with the UNH-IMEF model [*Matsui et al.*, 2008]. Here 5 min values of the model electric field are calculated using measured interplanetary parameters as an input to the model. The electric field as an output from the model is statistically analyzed in a similar manner as the measured field. As the model field is originally calculated at the magnetic equator, we have mapped the field values at in situ Cluster locations by using the dipole field [*Mozer*, 1970]. The mapping factor from the equator to the in situ locations is not so large and equals to 117% on average. Maximum electric field in the model in the nightside is ~2.5 mV/m for 5 min values, while ~0.7 mV/m for 6 h averages, both of which are smaller than our measurements: 12 mV/m for 5 min values and 2.5 mV/m for 6 h averages. There are reasons for the possible discrepancy between the measurement and the model. One reason is that an input parameter to the model, IEF, is beyond the valid range. Another is that more data during storm time are introduced in this study by increasing number of EFW data. A revision of the model with this new database will be considered in future.

[50] Electric field measurements in the duskside are partially made inside the inner edge of the electron plasma sheet (Figure 8). The E_Y component around the minimum *Dst* reported in section 3.1 is positively enhanced inside the inner edge. This positive enhancement could correspond to the undershielding [*Wolf*, 1983]. The E_Y component during the recovery phase is mostly positive in Figure 10c, indicating we cannot find the overshielding with a negative sign expected during this period. Another signature expected at this MLT is SAID. The E_Y component measured around zero epoch and during the recovery phase is 1–2 mV/m and <~1 mV/m, respectively. These values are not inconsistent with statistics of SAPS by *Foster and Vo* [2002] with typical values of >250 m/s since 1 mV/m of equatorial radial electric field at $L = 5$ corresponds to ~400 m/s of the drift velocity in the ionosphere.

[51] Electric fields are enhanced around zero epoch and decay after that in the morningside and dayside like those in the eveningside and nightside. The sizes for both 5 min and 6 h averages are comparable to those in the eveningside and the nightside. Further inter-sector comparison is not so easy because the number of events and IEF are different between each MLT sector. Nonetheless, one common feature is that E_Y is generally positive, indicating that plasma is transported sunward toward the magnetopause.

5.2. Decay of Electric Field Component During Recovery Phase

[52] Electric fields decay in time during the recovery phase as do the interplanetary and geomagnetic parameters (Figure 12). IMF B_Z recovers immediately after zero epoch. This is followed by IEF, *AL* index, and Cluster's electric field E_Y with decay time scales of 9–12 h. The longest decay times are found in *Dst*, *Kp*, and *AU* indices.

[53] It is hard to confirm different decay time between IEF and Cluster's E_Y. It is possible that both parameters are well related to each other. The efficiency is 0.11–0.15 at MLT ranges except duskside. This limits possible strength of DC electric field at Cluster's locations. When IEF takes extremely large values, the DC electric field may rather be limited because of the saturation effect.

[54] Short decay time of the Cluster's electric field compared to *Dst* index might indicate that the ring current does not necessarily enhance the electric field during the recovery phase. This is partly because ring current becomes symmetric and does not necessarily form a partial closed loop with the ionospheric current and electric fields. Vice versa, electric fields do not accelerate as many plasma sheet particles during the recovery phase, so that there are no more fresh plasma sheet particles to enhance ring current.

5.3. AC Components Relative to DC Components

[55] AC electric fields seen as standard deviations are large for fraction of periods as discussed in section 4.4.

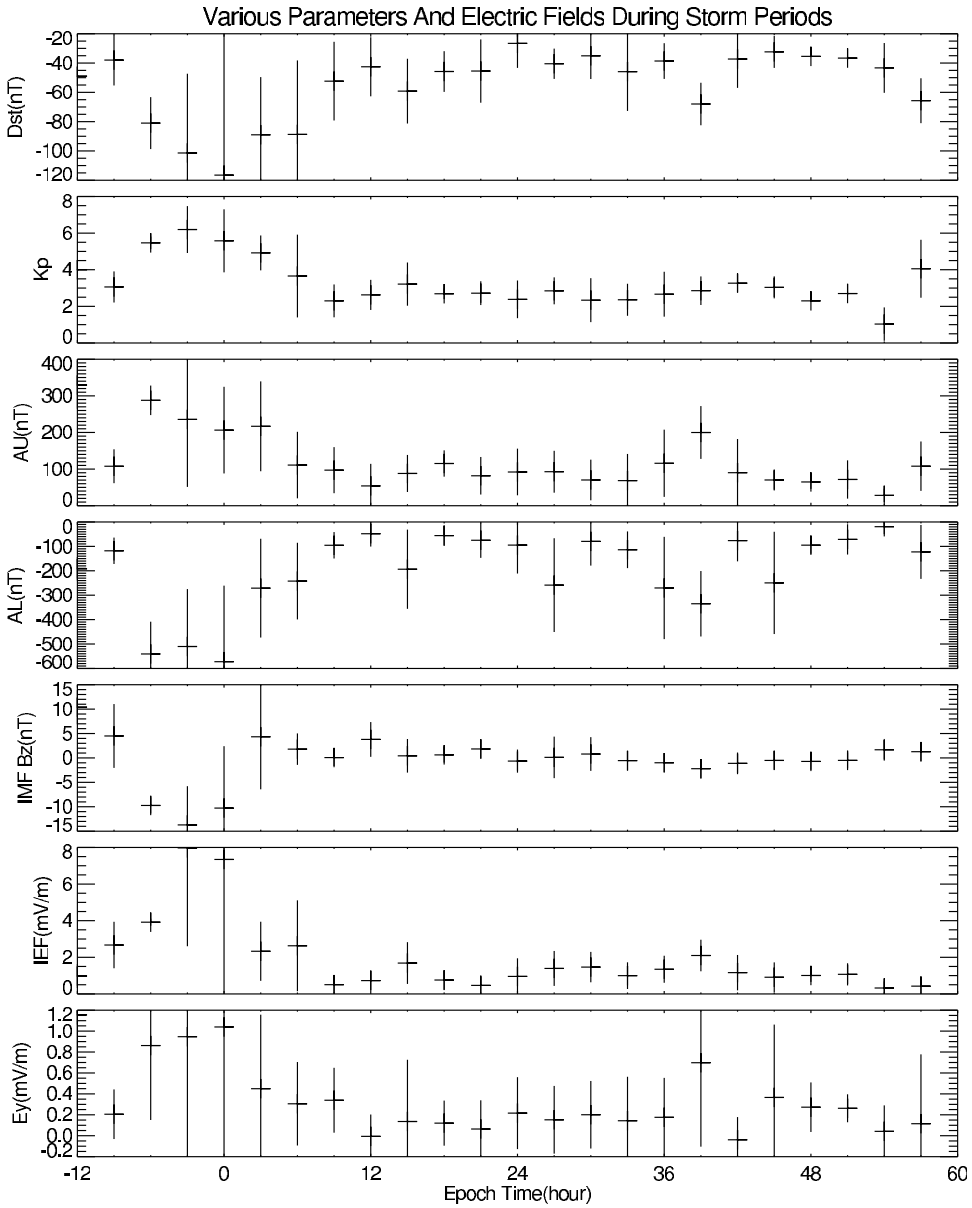

Figure 12. From top to bottom, superposed epoch analysis of following parameters are shown: *Dst*, *Kp*, *AU*, and *AL* indices, IMF B_Z component, IEF, and E_Y component measured by Cluster.

Standard deviations larger than several mV/m are sometimes found around zero epoch in the nightside. Some of them are shown to be inductive in the case study. DC field as identified by 6 h averages is often smaller than the standard deviations associated with AC components. It is therefore possible that variable and partly inductive components might play some role in accelerating ring current particles [*Li et al.*, 1998]. Our observation is not inconsistent with occurrence of bursty bulk flow in the magnetotail [*Baumjohann et al.*, 1990; *Angelopoulos et al.*, 1994], configuration of SMC events [*Sergeev et al.*, 1996], and Geotail observations during storm periods [*Hori et al.*, 2005]. Such signatures in the tail would also exist in the area investigated in this study. In terms of the plasma regime, Cluster is located outside the inner edge of the electron plasma sheet in the nightside around the main phase when electron data are available. This implies the magnetospheric electric field is not shielded at Cluster's locations.

5.4. Difference of Electric Fields Between Spacecraft

[56] We have measured different electric field profiles between spacecraft for an event on 18 February 2005. SC 2 and 3 located at outer L values likely measured inductive electric fields associated with dipolarization, while SC 1 and 4 located at inner side did not. There are three possibilities to explain this observation. First is that plasmapause where inductive fields would be reflected is located between inner spacecraft and outer spacecraft. This is unlikely at least comparing SC 1 and 3 because the EDI ambient electron data with an energy of 1 keV and a pitch angle of 90 degrees show continuous enhancement at both spacecraft, indicating they are located inside the electron plasma sheet. SC 2

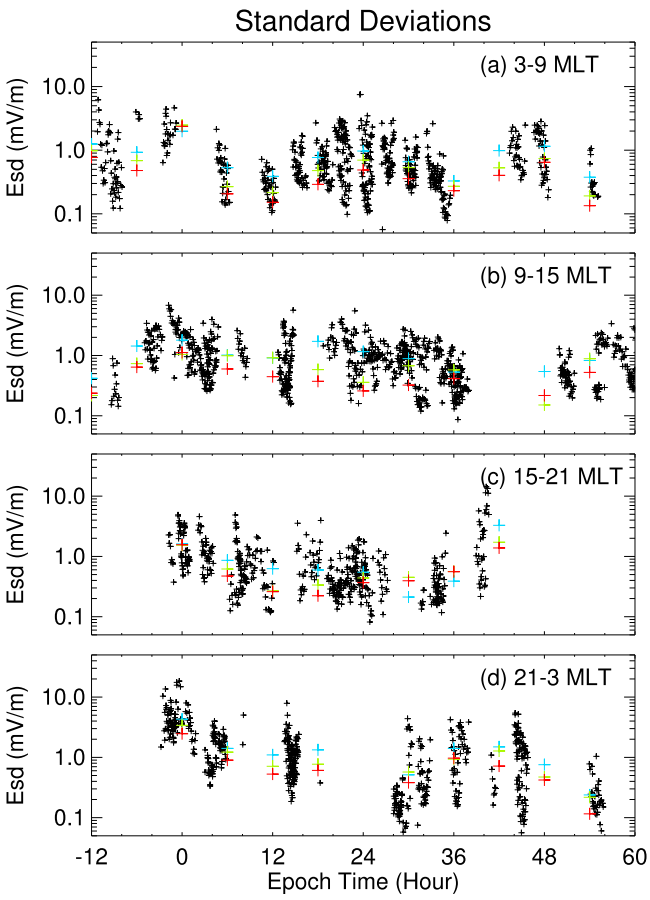

Figure 13. Standard deviations to calculate 5 min average electric fields from 4 s values shown with black points. Blue points are averages of the above standard deviations for each 6 h of epoch time. Green points are standard deviations to get 6 h averages in epoch time from 5 min electric fields. Red points show 6 h average values of electric fields to be compared with standard deviations. Each panel corresponds to different MLT: (a) 3–9 MLT, (b) 9–15 MLT, (c) 15–21 MLT, and (d) 21–3 MLT.

measured plasma sheet electrons at 500 eV with a pitch angle of 0 and 180 degrees. Similar observations are not available for SC 4. The second possibility is that magnetic elevation angle increase caused by dipolarization becomes insignificant as the background magnetic field enhances, which could be true. The third possibility is the dependence of measured electric field on MLT. MLT difference between outer two SC (SC 2 and 3) and inner two SC (SC 1 and 4) is ~0.1 h (Figure 6).

[57] Concerning subsequent large electric field without magnetic signatures, they are detected at all four spacecraft. The magnetic flux might therefore be transported inside the area of the region 1 current. It should be noted that the electric field corresponds to the rate of magnetic flux transport. In addition, dipolarization is expected to be related to enhancement of the region 1 current. Even the momentum of earthward plasma flow around the equator would not propagate to inner L value but to the ionosphere as region 1 current [*Shiokawa et al.*, 1998; *Birn et al.*, 1999], it is possible to have inward plasma flow inside region 1 current, which can be understood by conservation of magnetic flux. The flow speed or rate of magnetic flux transport might decrease at Cluster's location compared to that in the magnetotail because of accumulation of magnetic flux [*Baumjohann*, 2002; *Schödel et al.*, 2002]. Nonetheless, large electric field is sporadically observed in the inner magnetosphere because this region is not a rigid body. We do not know what is happening inside the electron plasma sheet in terms of shielding in the nightside because our present database does not cover this area. Cluster spacecraft started to decrease their perigee from middle of 2006, so that further expansion of the database may resolve this issue.

5.5. Variation of Electric Fields in the Premidnight During Storms

[58] We have measured different signs of E_X components depending on storm phase in the premidnight (Figure 10d). E_X is positive during the main phase, while it turns negative during the recovery phase. This could be related to spacecraft position relative to the location where convection pattern changes. The convection streamline is expected to be bending due to partial ring current [*C:son Brandt et al.*, 2002]. Figure 14 depicts a schematic cartoon of this convection streamline together with expected distribution of partial ring current. Such location with bending streamline might be closer to the Earth during the main phase, while it moves outward during the recovery phase.

[59] Next we move on to explain the spatial relation between the bending of the convection streamline and distribution of partial ring current. Recently *Gkioulidou et al.* [2009] explained the formation of this bending due to partial ring current, although they use a different term for this bending, namely Harang reversal. The trajectory of plasma sheet particles is dependent on energy due to different magnetic drifts. This causes higher-energy populations to be located in earlier MLT and outer L value than lower-energy populations. The pressure distribution of these populations

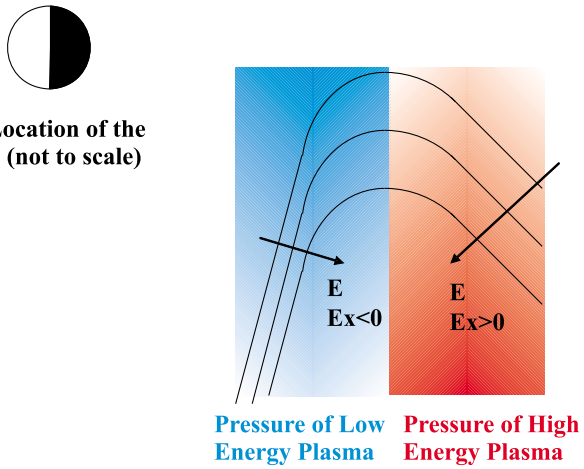

Figure 14. A cartoon of convection streamlines in the premidnight, which is consistent with our observation. Distributions of partial ring current are overlaid. Pressure distributions of high- and low-energy ions are shown by red and blue shades, respectively.

has azimuthal gradients, which causes generation of field-aligned current [*Vasyliunas*, 1970]. The polarity of this current depends on the direction of the gradient. In some MLTs, there is a discrepancy of the current polarity between the L value with high-energy particles and that with low-energy particles. This distribution of field-aligned currents together with the ionospheric condition basically causes the skewing of the convection streamline according to the simulation by *Gkioulidou et al.* [2009]. The pressure distributions of high-energy ions and low-energy ions are depicted with red and blue shades, respectively, in addition to the skewed convection streamline in Figure 14.

6. Conclusions

[60] Electric fields measured by Cluster at R = 3.5–6 R_E and $|MLAT| < 25$ degrees are investigated in this study during magnetic storms. First two event studies are reported. Both events are close to when the minimum value of *Dst* index is achieved. Large electric fields are observed during one event in the eveningside. Some of these large fields are likely to be related to undershielding and/or SAID. Large electric fields are also observed during another event in the nightside. The dipolarization signature is possibly accompanied by inductive electric fields at the outer two spacecraft, while this is not the case at the inner two spacecraft. A spatially variable feature of electric fields is therefore measured, which contributes to our statistical database. After the dipolarization, large electric field is observed by all spacecraft. As the electron counts are large, the spacecraft are outside the shielding layer, indicating that the electric field might not be attenuated at the spacecraft position. The electric field is possibly penetrating inside the region 1 current. We still do not know the behavior of electric fields inside the nightside region 2 current for lack of measurements. There are three events in the nightside around the minimum *Dst* including the event studied here. All events show decreasing *AL* index and increasing magnetic elevation.

[61] Then we have performed a superposed epoch analysis with zero epoch at minimum *Dst* using 71 storms. Electric field is enhanced around zero epoch at all MLTs and then decays during the recovery phase. Although the values in the morningside and dayside were not much investigated previously, they are actually enhanced around zero epoch. The enhanced electric field in the eveningside partly corresponds to the SAID. The large electric field during the main phase in the nightside is partly inductive. The values are somewhat smaller than previous measurements in the inner magnetosphere possibly caused by limited coverage of spacecraft locations. The measurement is consistent with those performed in the magnetotail. The size of the electric field is larger than that estimated in our previous model, indicating possible improvement required for the model. We have found changes of E_X signs in the premidnight between the main and recovery phases, possibly indicating shift of locations with bending of convection streamline related to partial ring current. The decay time scale of Cluster's E_Y components is comparable to those of *AL* index and IEF. This is shorter than *Dst* index but longer than IMF B_Z. It is possible that the electric field decay during the recovery phase precedes the decay of the ring current. In this case, the ring current is more symmetric because of trapping of energetic ions on closed drift paths; this leads to smaller connection with the ionospheric current and electric field. We have calculated the ratio between E_Y components and IEF. The values are 0.11–0.15 except in the eveningside, where the ratio is larger. The saturation of this ratio is found for one event. The size of DC electric field in the inner magnetosphere might thus have an upper limit. AC electric field is occasionally enhanced in our analysis. The size is larger than that of DC component. AC components therefore might contribute to accelerate ring current particles.

[62] Following topics are still not investigated in our study: statistical relation between electric field and other quantities measured by Cluster such as magnetic field, measurements at other spatial locations particularly closer to the Earth, and similar type of analysis using data from other spacecraft. By including results from the present study as well as the above future studies, we would like to improve our empirical electric field model.

[63] **Acknowledgments.** We thank the reviewers for the useful comments to improve the manuscript. Helpful discussions with M. F. Thomsen and J. Goldstein are acknowledged. EFW data are provided through Cluster Active Archive. We would like to thank N. F. Ness and D. J. McComas for ACE MAG and SWEPAM data, respectively. Both data are obtained from NASA CDA Website. *Dst*, *AL*, *AU*, and *SYM-H* indices are provided by World Data Center at Kyoto University. This work was supported by NASA grants NNX07AI03G and NNG05GG25G.

[64] Masaki Fujimoto thanks the reviewers for their assistance in evaluating this paper.

References

Anderson, P. C., D. L. Carpenter, K. Tsuruda, T. Mukai, and F. J. Rich (2001), Multisatellite observations of rapid subauroral ion drifts (SAID), *J. Geophys. Res.*, *106*(A12), 29,585–29,599, doi:10.1029/2001JA000128.

Angelopoulos, V., W. Baumjohann, C. F. Kennel, F. V. Coroniti, M. G. Kivelson, R. Pellat, R. J. Walker, H. Lühr, and G. Paschmann (1992), Bursty bulk flows in the inner central plasma sheet, *J. Geophys. Res.*, *97*(A4), 4027–4039, doi:10.1029/91JA02701.

Angelopoulos, V., et al. (1994), Statistical characteristics of bursty bulk flow events, *J. Geophys. Res.*, *99*(A11), 21,257–21,280, doi:10.1029/94JA01263.

Balogh, A., et al. (2001), The Cluster Magnetic field investigation: Overview of in-flight performance and initial results, *Ann. Geophys.*, *19*, 1207–1217.

Baumjohann, W. (2002), Modes of convection in the magnetotail, *Phys. Plasmas*, *9*, 3665–3667.

Baumjohann, W., G. Haerendel, and F. Melzner (1985), Magnetospheric convection observed between 0600 and 2100 LT: Variations with *Kp*, *J. Geophys. Res.*, *90*(A1), 393–398, doi:10.1029/JA090iA01p00393.

Baumjohann, W., G. Paschmann, and H. Lühr (1990), Characteristics of high-speed ion flows in the plasma sheet, *J. Geophys. Res.*, *95*(A4), 3801–3809, doi:10.1029/JA095iA04p03801.

Baumjohann, W., Y. Kamide, and R. Nakamura (1996), Substorms, storms, and the near-Earth tail, *J. Geomag. Geoelectr.*, *48*, 177–185.

Birn, J., M. Hesse, G. Haerendel, W. Baumjohann, and K. Shiokawa (1999), Flow braking and the substorm current wedge, *J. Geophys. Res.*, *104*(A9), 19,895–19,903, doi:10.1029/1999JA900173.

Blanc, M., and G. Caudal (1985), The spatial distribution of magnetospheric convection electric fields at ionospheric altitudes: A review: 2. Theories, *Ann. Geophys.*, *3*, 27–42.

Carpenter, D. L., B. L. Giles, C. R. Chappell, P. M. E. Décréau, R. R. Anderson, A. M. Persoon, A. J. Smith, Y. Corcuff, and P. Canu (1993), Plasmasphere dynamics in the duskside bulge region: A new look at old topic, *J. Geophys. Res.*, *98*(A11), 19,243–19,271, doi:10.1029/93JA00922.

C:son Brandt, P., S. Ohtani, D. G. Mitchell, M.-C. Fok, E. C. Roelof, and R. Demajistre (2002), Global ENA observations of the storm mainphase ring current: Implications for skewed electric fields in the inner magnetosphere, *Geophys. Res. Lett.*, *29*(20), 1954, doi:10.1029/2002GL015160.

Dungey, J. W. (1961), Interplanetary magnetic field and the auroral zones, *Phys. Rev. Lett.*, *2*, 47–48.

Ejiri, M. (1978), Trajectory traces of charged particles in the magnetosphere, *J. Geophys. Res.*, *83*(A10), 4798–4810, doi:10.1029/JA083iA10p04798.

Escoubet, C. P., M. Fehringer, and M. Goldstein (2001), The Cluster mission, *Ann. Geophys.*, *19*, 1197–1200.

Fejer, B. G., and L. Scherliess (1997), Empirical models of storm time equatorial zonal elecric fields, *J. Geophys. Res.*, *102*(A11), 24,047–24,056, doi:10.1029/97JA02164.

Förster, M., G. Paschmann, S. E. Haaland, J. M. Quinn, R. B. Torbert, H. Vaith, and C. A. Kletzing (2007), High-latitude plasma convection from Cluster EDI: Variances and solar wind correlations, *Ann. Geophys.*, *25*, 1691–1707.

Foster, J. C. (1993), Storm-time plasma transport at middle and high latitudes, *J. Geophys. Res.*, *98*(A2), 1675–1689, doi:10.1029/92JA02032.

Foster, J. C., and W. J. Burke (2002), Saps: A new categorization for subauroral electric fields, *EOS Trans. AGU*, *83*(36), 393–394.

Foster, J. C., and H. B. Vo (2002), Average characteristics and activity dependence of the subauroral polarization stream, *J. Geophys. Res.*, *107*(A12), 1475, doi:10.1029/2002JA009409.

Galperin, Y. I., V. N. Ponomarev, and A. G. Zosimova (1974), Plasma convection in polar ionosphere, *Ann. Geophys.*, *30*, 1–7.

Garner, T. W., R. A. Wolf, R. W. Spiro, W. J. Burke, B. G. Fejer, S. Sazykin, J. L. Roeder, and M. R. Hairston (2004), Magnetospheric electric fields and plasma sheet injection to low l shells during the 4–5 June 1991 magnetic storm: Comparison between the Rice Convection Model and observations, *J. Geophys. Res.*, *109*, A02214, doi:10.1029/2003JA010208.

Gkioulidou, M., C.-P. Wang, L. R. Lyons, and R. A. Wolf (2009), Formation of the Harang reversal and its dependence on plasma sheet conditions: Rice convection model simulations, *J. Geophys. Res.*, *114*, A07204, doi:10.1029/2008JA013955.

Goldstein, J., J. L. Burch, B. R. Sandel, S. B. Mende, P. C. Brandt, and M. R. Hairston (2005), Coupled response of the inner magnetosphere and ionosphere on 17 April 2002, *J. Geophys. Res.*, *110*, A03205, doi:10.1029/2004JA010712.

Gustafsson, G., et al. (2001), First results of electric field and density observations by Cluster EFW based on initial months of operation, *Ann. Geophys.*, *19*, 1219–1240.

Haaland, S. E., G. Paschmann, M. Förster, J. M. Quinn, R. B. Torbert, C. E. McIlwain, H. Vaith, P. A. Puhl-Quinn, and C. A. Kletzing (2007), High-latitude plasma convection from cluster edi measurements: Method and IMF dependence, *Ann. Geophys.*, *25*, 239–253.

Hairston, M. R., T. W. Hill, and R. A. Heelis (2003), Observed saturation of the ionospheric polar cap potential during the 31 March 2001 storm, *Geophys. Res. Lett.*, *30*(6), 1325, doi:10.1029/2002GL015894.

Hori, T., et al. (2005), Storm-time convection electric field in the near-Earth plasma sheet, *J. Geophys. Res.*, *110*, A04213, doi:10.1029/2004JA010449.

Jordanova, V. K., Y. S. Miyoshi, S. Zaharia, M. F. Thomsen, G. D. Reeves, D. S. Evans, C. G. Mouikis, and J. F. Fennell (2006), Kinetic simulations of ring current evolution during the geospace environment modelling challenge events, *J. Geophys. Res.*, *111*, A11S10, doi:10.1029/2006JA011644.

Jordanova, V. K., H. Matsui, P. A. Puhl-Quinn, M. F. Thomsen, K. Mursula, and L. Holappa (2009), Ring current development during high-speed streams, *J. Atmos. Sol. Terr. Phys.*, *71*, 1093–1102, doi:10.1016/j.jastp.2008.09.043.

Kamide, Y., et al. (1998), Current understanding of magnetic storms: Storm-substorm relationships, *J. Geophys. Res.*, *103*(A8), 17,705–17,728, doi:10.1029/98JA01426.

Khotyaintsev, Y., P.-A. Lindqvist, A. I. Eriksson, and M. André (2010), The EFW Data in the CAA, in *The Cluster Active Archive, Studying the Earth's Space Plasma Environment*, *Astrophys. Space Sci. Proc.*, edited by H. Laakso, M. G. T. T. Taylor, and C. P. Escoubet, pp. 97–108, Springer, Berlin.

Kistler, L. M., F. M. Ipavich, D. C. Hamilton, G. Gloeckler, B. Wilken, G. Kremser, and W. Stüdemann (1989), Energy spectra of the major ion species in the ring current during gomagnetic storms, *J. Geophys. Res.*, *94*(A4), 3579–3599, doi:10.1029/JA094iA04p03579.

Lemaire, J. F., and K. I. Gringauz (1998), *The Earth's Plasmasphere*, Cambridge Univ. Press, New York.

Li, X., D. N. Baker, M. Temerin, G. D. Reeves, and R. D. Belian (1998), Simulation of dispersionless injections and drift echoes of energetic electrons associated with substorms, *Geophys. Res. Lett.*, *25*(20), 3763–3766, doi:10.1029/1998GL900001.

Lindqvist, P.-A., Y. Khotyaintsev, M. André, and A. I. Eriksson (2006), EFW data in the Cluster Active Archive, paper presented at Cluster and Double Star Symposium, ESA, Noordwijk, Neth., 19–23 September.

Lui, A. T. Y., R. W. McEntire, and K. B. Baker (2001), A new insight on the cause of magnetic storms, *Geophys. Res. Lett.*, *28*(17), 3413–3416, doi:10.1029/2001GL013281.

Matsui, H., J. M. Quinn, R. B. Torbert, V. K. Jordanova, W. Baumjohann, P. A. Puhl-Quinn, and G. Paschmann (2003), Electric field measurements in the inner magnetosphere by Cluster EDI, *J. Geophys. Res.*, *108*(A9), 1352, doi:10.1029/2003JA009913.

Matsui, H., P. A. Puhl-Quinn, V. K. Jordanova, Y. Khotyaintsev, P.-A. Lindqvist, and R. B. Torbert (2008), Derivation of inner magnetospheric electric field (unh-imef) model using cluster data set, *Ann. Geophys.*, *26*, 2887–2898.

Maynard, N. C., T. L. Aggson, and J. P. Heppner (1983), The plasmaspheric electric field as measured by ISEE 1, *J. Geophys. Res.*, *88*(A5), 3981–3990, doi:10.1029/JA088iA05p03991.

McComas, D. J., S. J. Bame, P. Baker, W. C. Feldman, J. L. Phillips, P. Riley, and J. W. Griffee (1998), Solar wind electron proton alpha monitor (SWEPAM) for the advanced composition explorer, *Space Sci. Rev.*, *86*, 563–612.

Mozer, F. S. (1970), Electric field mapping in the ionosphere at the equatorial plane, *Planet. Space Sci.*, *18*, 259–263.

Nishimura, Y., J. Wygant, T. Ono, M. Iizima, A. Kumamoto, D. Brautigam, and R. Friedel (2008), SAPS measurements around the magnetic equator by CRRES, *Geophys. Res. Lett.*, *35*, L10104, doi:10.1029/2008GL033970.

Ohtani, S., et al. (2007), Cluster observations in the inner magnetosphere during the 18 April 2002 sawtooth event: Dipolarization and injection at $r = 4.6r_e$, *J. Geophys. Res.*, *112*, A08213, doi:10.1029/2007JA012357.

Okada, T., H. Hayakawa, K. Tsuruda, A. Nishida, and A. Matsuoka (1993), EXOS D observations of enhanced electric fields during the giant magnetic storm in March 1989, *J. Geophys. Res.*, *98*(A9), 15,417–15,424, doi:10.1029/93JA01128.

Paschmann, G., et al. (2001), The Electron Drift Instrument on Cluster: Overview of first results, *Ann. Geophys.*, *19*, 1273–1288.

Peymirat, C., A. D. Richmond, and A. T. Kobea (2000), Electrodynamic coupling of high and low latitudes: Simulations of shielding/overshielding effects, *J. Geophys. Res.*, *105*(A10), 22,991–23,003, doi:10.1029/2000JA000057.

Puhl-Quinn, P. A., H. Matsui, E. Mishin, C. Mouikis, L. Kistler, Y. Khotyaintsev, P. M. E. Décréau, and E. Lucek (2007), Cluster and DMSP observations of SAID electric fields, *J. Geophys. Res.*, *112*, A05219, doi:10.1029/2006JA012065.

Puhl-Quinn, P. A., H. Matsui, V. K. Jordanova, Y. Khotyaintsev, and P.-A. Lindqvist (2008), An effort to derive an empirically based, inner-magnetospheric electric field model: Merging Cluster EDI and EFW data, *J. Atmos. Sol. Terr. Phys.*, *70*, 564–573.

Roederer, J. G. (1970), *Dynamics of Geomagnetically Trapped Radiation*, Springer, New York.

Rowland, D. E., and J. R. Wygant (1998), Dependence of the large-scale, inner magnetospheric electric field on geomagnetic activity, *J. Geophys. Res.*, *103*(A7), 14,959–14,964, doi:10.1029/97JA03524.

Schödel, R., K. Dierschke, W. Baumjohann, R. Nakamura, and T. Mukai (2002), The storm time central plasma sheet, *Ann. Geophys.*, *20*, 1737–1741.

Sergeev, V. A., R. J. Pellinen, and T. I. Pulkkinen (1996), Steady magnetospheric convection: A review of recent results, *Space Sci. Rev.*, *75*, 551–604.

Shiokawa, K., G. Haerendel, and W. Baumjohann (1998), Azimuthal pressure gradient as driving force of substorm currents, *Geophys. Res. Lett.*, *25*(7), 959–962, doi:10.1029/98GL00540.

Smith, C. W., J. L'Heureux, N. F. Ness, M. H. Acuña, L. F. Burlaga, and J. Scheifele (1998), The ACE magnetic fields experiment, *Space Sci. Rev.*, *86*, 613–632.

Southwood, D. J., and R. A. Wolf (1978), An assessment of the role of precipitation in magnetospheric convection, *J. Geophys. Res.*, *83*(A11), 5227–5232, doi:10.1029/JA083iA11p05227.

Vasyliunas, V. M. (1970), Mathematical models of magnetospheric convection and its coupling to the ionosphere, in *Particles and Fields in the Magnetosphere*, edited by B. M. McCormac, pp. 60–71, D. Reidel, Dordrecht, Netherlands.

Vasyliunas, V. M. (1972), The interrelationship of magnetospheric processes, in *Earth's Magnetospheric Processes*, edited by B. M. McCormac, pp. 29–38, D. Reidel, Dordrecht, Netherlands.

Wing, S., and D. G. Sibeck (1997), Effects of interplanetary magnetic field *z* component and the solar wind dynamic pressure on the geosynchronous magnetic field, *J. Geophys. Res.*, *102*(A4), 7207–7216, doi:10.1029/97JA00150.

Wolf, R. A. (1983), The quasi-static (slow-flow) region of the magnetosphere, in *Solar-Terrestrial Physics*, edited by R. L. Carovillano and J. M. Forbes, pp. 303–368, D. Reidel, Dordrecht, Netherlands.

Wygant, J., D. Rowland, H. J. Singer, M. Temerin, F. Mozer, and M. K. Hudson (1998), Experimental evidence on the role of the large spatial scale electric field in creating the ring current, *J. Geophys. Res.*, *103*(A12), 29,527–29,544, doi:10.1029/98JA01436.

Yeh, H.-C., J. C. Foster, F. J. Rich, and W. Swider (1991), Storm time electric field penertration observed at midlatitude, *J. Geophys. Res.*, *96*(A4), 5707–5721, doi:10.1029/90JA02751.

Zhang, J., M. W. Liemohn, J. U. Kozyra, M. F. Thomsen, H. A. Elliott, and J. M. Weygand (2006), A statistical comparison of solar wind sources of moderate and intense geomagnetic storms at solar minimum and maximum, *J. Geophys. Res.*, *111*, A01104, doi:10.1029/2005JA011065.

Zong, Q.-G., et al. (2009), Vortex-like plasma flow structures observed by cluster at the boundary of the outer radiation belt and ring current: A link between the inner and outer magnetosphere, *J. Geophys. Res.*, *114*, A10211, doi:10.1029/2009JA014388.

J. W. Bonnell, Space Sciences Laboratory, University of California, Berkeley, CA 94720, USA.

C. J. Farrugia, H. Matsui, and R. B. Torbert, Space Science Center, University of New Hampshire, 8 College Road, Durham, NH 03824, USA. (hiroshi.matsui@unh.edu)

E. Georgescu, Max-Planck-Institut für Sonnensystemforschung, D-37191 Katlenburg-Lindau, Germany.

V. K. Jordanova, Los Alamos National Laboratory, Los Alamos, NM 87545, USA.

Yu. V. Khotyaintsev, Swedish Institute of Space Physics, Box 537, SE-75121 Uppsala, Sweden.

P.-A. Lindqvist, Alfvén Laboratory, Royal Institute of Technology, SE-10044 Stockholm, Sweden.

P. A. Puhl-Quinn, AER, Inc., 131 Hartwell Ave., Lexington, MA 02421, USA.